

Oscillatory tunneling between quantum Hall systems

Tin-Lun Ho

*Physics Department, The Ohio State University, Columbus, Ohio, 43210,**
National High Magnetic Field Laboratory, Florida State University, Tallahassee, Florida 32306-4005;
Physics Department, Hong Kong University of Science and Technology, Clear Water Bay, Kowloon, Hong Kong;
and Physics Department, Chinese University of Hong Kong, Shatin, New Territory Hong Kong
 (Received 11 March 1994)

Electron tunneling between quantum Hall systems on the same two-dimensional plane separated by a narrow barrier is studied. We show that in the limit where the inelastic scattering time is much longer than the tunneling time, which can be achieved in practice, electrons can tunnel back and forth through the barrier continuously, leading to an oscillating current in the absence of external drives. The oscillatory behavior is dictated by a tunneling gap in the energy spectrum. We shall discuss ways to generate oscillating currents and the phenomenon of natural dephasing between the tunneling currents of edge states. The noise spectra of these junctions are also studied. They contain singularities reflecting the existence of tunneling gaps as well as the inherent oscillation in the system.

I. OSCILLATORY TUNNELING IN QUANTUM HALL SYSTEMS

In this paper we study electron tunneling between quantum Hall (QH) systems separated by *thin* barriers. Examples of these systems are shown in Figs. 1–6. The thinness of the barrier allows an electron to tunnel through it many times before being scattered away by inelastic effects. Oscillatory tunneling of this kind will occur if the inelastic scattering time τ_{in} is much longer than the tunneling time τ_T ,

$$\tau_{in} \gg \tau_T. \tag{1}$$

The existence of oscillatory tunneling can be seen even in the semiclassical (SC) limit, where electron wave packets move in circular orbits with cyclotron frequency ω_c . When the barrier is infinite, electrons will undergo a sequence of “reflected circular orbits” as shown in Fig. 1. In the absence of other scattering mechanism, electrons having collided with the barrier once must collide with it again within the cyclotron period. As a result, they are

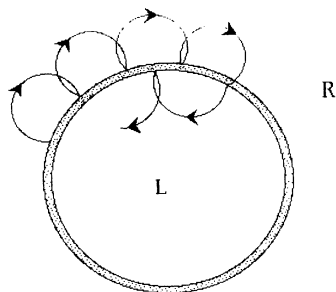


FIG. 1. A quantum Hall junction with a circular barrier. The trajectory of a semiclassical electron is indicated by arrows. Once tunneled across the barrier, the electron will repeat a similar reflected circular motion on the other side and eventually tunnel back.

forever *captured* by the barrier (see Fig. 6). When the barrier is reduced from infinity to a finite value, the *captured* electrons on one side of the barrier (say, *L*) can tunnel to the other side (*R*). Once tunneled, this electron will collide repeatedly with the barrier and eventually tunnel back to *L*. When Eq. (1) is satisfied, this back and forth tunneling process can proceed without interruption, giving rise to an oscillating current in the absence of external drives.

While the SC picture captures the correct physics, it only tells half the story. In a quantum-mechanical treatment, we shall see that different edge states tunnel with different frequencies. Thus, even in the absence of inelastic scattering, the tunneling current of different edge states will naturally dephase with each other. As a result, the total tunneling current will decrease in time. However, we show later that despite dephasing effects, there are ways to generate lasting current oscillations (thereby reflecting the oscillatory tunneling near the barrier) without the aid of an ac drive.

The crucial question is whether Eq. (1) can be

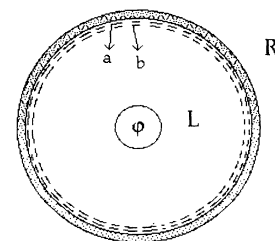


FIG. 2. Schematic representation of the quantum-mechanical edge states near the barrier. The dotted lines labeled *a* and *b* denote two neighboring edge states, which in general have different tunneling rates across the barrier. As the flux ϕ through the hole at the center increases, the edge states will move outward, thereby increasing their tunneling rates. State *b* will evolve to *a* when $\phi = 2\pi$.

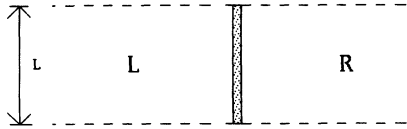


FIG. 3. A rectangular version of the QH junction in Fig. 1. The dashed lines mean that the system is periodic in y with period L .

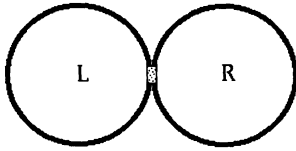


FIG. 4. A quantum Hall weak link. The thick black lines represent hard walls, i.e., infinite potentials. As we shall see, oscillatory tunneling of the electrons across the weak link produces a singularity in the noise of the tunneling current.

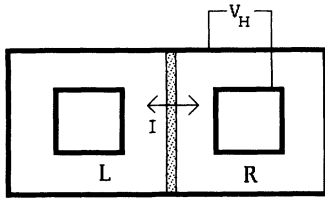


FIG. 5. A junction similar to Fig. 4 except that both R and L are multiply connected geometries. The current oscillation across the junction will generate an oscillation of Hall voltage across each ring.

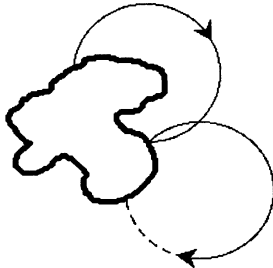


FIG. 6. In the absence of external electric fields, a semiclassical electron will be forever captured by the barrier once its trajectory is intercepted by it.

achieved. We shall argue below that this is possible at least for the case of integer filling. There are two sources of inelastic scattering: Coulomb interaction between electrons on the same side of the barrier (“intra-region” interaction) and that on the different sides (“inter-region” interaction). Let us first consider noninteracting electrons and the limit of infinite barrier. The systems R and L on both sides of the barrier are now disconnected, reducing to two semi-infinite systems terminated by a hard wall. The Landau levels of such systems are well known, i.e., they bend upward as the barrier is approached,^{1,2} see Fig. 7. In the presence of intraregion interaction (but without inter-region interaction), and when the system has integer filling, the edge electrons will behave like a normal Fermi liquid.³ The lifetime τ_{in} of the quasiparticles will tend to infinity at the Fermi surface, and will dominate over any tunneling time τ_T introduced by finite barriers. In other words, Eq. (1) can always be satisfied near the Fermi surface when the system has integer filling, and that electron tunneling near the Fermi surface can be modeled by that of noninteracting systems. (Estimates of the tunneling time are given at the end of the paper.) As we have seen in Fig. 7, the Landau levels of R and L intersect because they all bend upward near the barrier. In the presence of tunneling, these intersections will turn into gaps (see Fig. 8). As we shall see, the unusual features of these junctions are determined by these gaps.

What is more subtle is the effect of inter-region interactions. While it is obvious that the tunneling gap can sufficiently withstand weak inter-region interactions, the situation is less clear for large inter-region interactions. However, as we will show later, it is possible to map our problem to a solvable model in one dimension (massive Thirring model). The exact solution of this model shows that the tunneling gap exists for arbitrary inter-region interaction. Although we have not yet been able to calculate the current responses for arbitrary inter-region in-

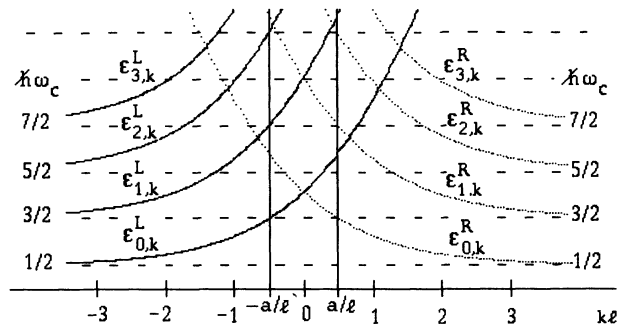


FIG. 7. The spectrum of the rectangular QH system in Fig. 3 in the infinite barrier limit (Refs. 1 and 2). Because of translational invariance in y , the spectrum can be labeled by the y momentum k and the Landau level index n . The width of the barrier is $2a$. Its boundaries are denoted in dimensionless units $(-a/l, a/l)$, where l is the magnetic length. The spectra of L and R , $\epsilon_{n,k}^L$ and $\epsilon_{n,k}^R$ are represented by solid and dashed curves. They rise near the barrier (i.e., $|k| \rightarrow 0$) and intersect each other. See also Sec. II for a detailed discussion.

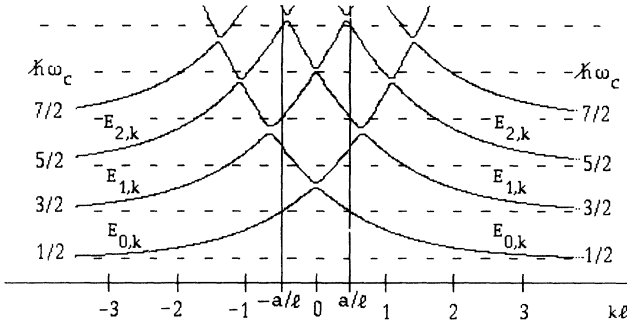


FIG. 8. The intersections of the spectra in Fig. 7 turn into gaps as the infinite barrier becomes finite. The spectrum of the entire system will be denoted as $E_{n,k}$. They are continuous curves that reduce to $\epsilon_{n,k}^L$ and $\epsilon_{n,k}^R$ as one approaches the bulk, i.e., as $k \ll -l^{-1}$ and $k \gg l^{-1}$, where l is the magnetic length.

teraction, the survival of the tunneling gap suggests that the tunneling characteristics of the noninteracting systems may also survive.

Before proceeding, we stress that the phenomena discussed here requires thin barriers. The junction used in many current experiments are produced by gate voltages and are much smoother than the barriers we consider here.⁴ Since magnetic length in a 10-T field is about 80 Å, and the 100-Å-wide channels are feasible in current technology, the construction of these junctions is possible (see also Sec. VII for estimates of relevant parameters).

The rest of the paper is organized as follows. In Sec. II, we discuss the energy spectra in the vicinity of the barrier for a variety of external conditions. In Sec. III, we derive the effective Hamiltonian for the tunnel junction as well as the expression of tunneling current. In Sec. IV, we suggest ways to generate oscillatory tunneling currents, and discuss the phenomenon of natural dephasing. In Sec. V, we discuss the noise spectrum of the junction, which reflects directly the existence of tunneling gaps and the inherent natural oscillations of the system. In Sec. VI, we discuss the effect of inter-region Coulomb interaction. In Sec. VII, we give numerical estimates of various parameters.

II. THE ENERGY SPECTRUM NEAR THE BARRIER

We have argued in Sec. I that when Eq. (1) is satisfied, tunneling between QH systems with fully filled Landau levels can be modeled by that of noninteracting electrons. Although we have mentioned the general behavior of the spectrum in Sec. I, we shall give a detailed description here as we shall need it later. For simplicity, we shall focus on the setup in Fig. 3. The system is periodic in y , $\psi(x, y) = \psi(x, y + L)$. The Hamiltonian in the Landau gauge is

$$H = \frac{1}{2m} p_x^2 + \frac{1}{2m} \left[p_y - \frac{e}{c} Bx \right]^2 + V(x), \quad (2)$$

where B is the external magnetic field, and $V(x) = V_0 < 0$ or 0 for $|x| < a$ or $|x| > a$ (see Fig. 7). The eigenstates are of the form $\psi_{n,k}(x, y) = L^{-1/2} e^{iky} u_{n,k}(x)$, $k = (2\pi m)/L$,

where m is an integer and $u_{n,k}(x)$ is an eigenfunction of

$$H_k(x) = \hbar\omega_c \left[-\frac{1}{2} l^2 \partial_x^2 + V_k(x) \right], \quad (3)$$

$$V_k(x) \equiv \frac{1}{2} \left[\frac{x}{l} - kl \right]^2 + V(x)/\hbar\omega_c,$$

with energy $E_{n,k}$. Here, $l = \sqrt{\hbar c/eB}$ is the magnetic length and $\omega_c = (eB/mc)$ is the cyclotron frequency. Equation (2) can be written as

$$H = \sum_k H_k \equiv \sum_k \sum_{n=0}^{\infty} E_{n,k} a_{n,k}^+ a_{n,k}, \quad (4)$$

where $a_{n,k}$ is the annihilation operator of $\psi_{n,k}$. The existence of oscillatory tunneling near the barrier can be seen from the fact that $V_k(x)$ reduces to a degenerate double well as $k \rightarrow 0$. It is well known that when an electron is placed in one side of the double well, it will tunnel back and forth between the wells with a frequency given by the excitation energy from the ground state to the first excited state.

Although both $u_{n,k}(x, y)$ and $E_{n,k}$ can be obtained by analytic methods,² they can be easily understood in the limit of high barriers. When $V_0 = \infty$, L and R become two disconnected semi-infinite systems, $H \rightarrow H_L + H_R$,

$$H_L = \sum_{k=0}^{\infty} \sum_{n=0}^{\infty} \epsilon_{n,k}^L c_{n,k}^+ c_{n,k}, \quad (5)$$

$$H_R = \sum_{k=0}^{\infty} \sum_{n=0}^{\infty} \epsilon_{n,k}^R d_{n,k}^+ d_{n,k},$$

where $\epsilon_{n,k}^L$ and $\epsilon_{n,k}^R$ are the Landau levels of L and R in the limit $V_0 = \infty$. $c_{n,k}$ and $d_{n,k}$ are the corresponding eigenstates. The behavior of the Landau levels $\epsilon_{n,k}^L$ and $\epsilon_{n,k}^R$ as a function of k have been studied by a number of authors^{1,2} (see also Figs. 7 and 8). In the bulk of L , $lk \ll -1$, $\epsilon_{n,k}^L = (n + 1/2)\hbar\omega_c$. $\epsilon_{n,k}^L$ begins to deviate appreciably from its bulk value about a magnetic length away from the wall, $lk \approx -1$. The entire curve increases monotonically (to infinity) as k increases, passing through $(2n + 3/2)\hbar\omega_c$ at the barrier (i.e., when $lk = -a/l$). $\epsilon_{n,k}^R$ has an identical behavior in the reverse k direction. When V_0 is reduced from infinity to a finite value, the intersections of the spectra of L and R will turn into ‘‘tunneling’’ gaps. The two sets of energy curves $\{\epsilon_{n,k}^L\}$ and $\{\epsilon_{n,k}^R\}$ now turn into a single set $\{E_{n,k}\}$, which we shall refer to as the n -th Landau level of the entire system. Each curve $E_{n,k}$ is a smooth function in k . It reduces to $\epsilon_{n,k}^L$ and $\epsilon_{n,k}^R$ for $lk \ll -1$ and $lk \gg 1$.

The qualitative features of the wave functions $u_{n,k}$ can be determined from the effective potential $V_k(x)$ (see Fig. 9). If $\phi_{n,k}^L(x)$ and $\phi_{n,k}^R(x)$ are the eigenstates of L and R in the infinite barrier limit [hence $\phi_{n,k}^L(x) = 0$ for $x > 0$, and $\phi_{n,k}^R(x) = 0$ for $x < 0$], then for high (but finite) barriers, we have (see Fig. 9).

$$u_{0(1),k} \approx [\phi_{0,k}^L(x) + (-)\phi_{0,k}^R(x)]/\sqrt{2} \quad \text{for } -1 \ll lk \ll 1, \quad (6)$$

$$u_{0(1),k}(x) \approx \phi_{0(1),k}^L(x) \quad \text{for } lk \ll -1, \quad (7)$$

$$u_{0(1),k}(x) \approx \pm \phi_{0(1),k}^R(x) \quad \text{for } lk \gg 1. \quad (8)$$

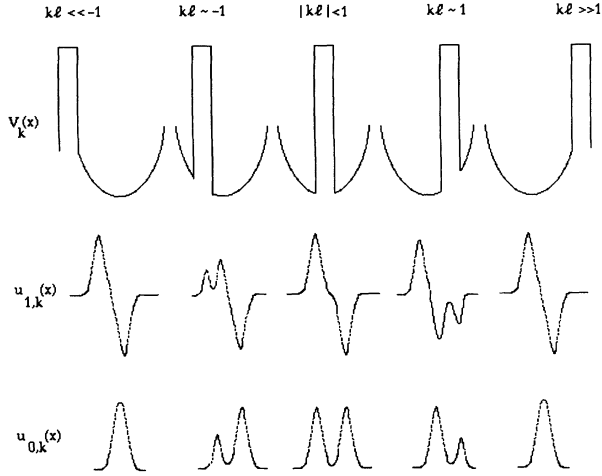


FIG. 9. A schematic representation of the wave functions of the ground state $u_{0,k}(x)$ and first excited state $u_{1,k}(x)$ of the entire system $L+R$ in Fig. 8.

In the absence of voltage bias between L and R , it can be seen from Fig. 8 that the lowest tunneling gap of L and R (which occurs at $k=0$) lie above the first “bulk” Landau level, i.e., $(\frac{3}{2})\hbar\omega_c$. The location of the tunneling gap, however, can be easily changed by applying a voltage bias (see Fig. 10). Note that in the presence of a voltage bias V , H is still diagonal in k and is still given by Eq. (5) except that the spectrum $E_{n,k}$ and the eigenstates $a_{n,k}$ now functions of V .

When the spins of the electrons are taken into account, the spectrum of L and R in the infinite barrier limit consists of two sets of Landau levels differing from each other by the Zeeman energy. Since $V(x)$ does not flip spins, the intersections of the opposite spin Landau levels will not turn into gaps when V_0 becomes finite.

To conclude this section, we derive the expression for the current in the x direction. If we define the number of

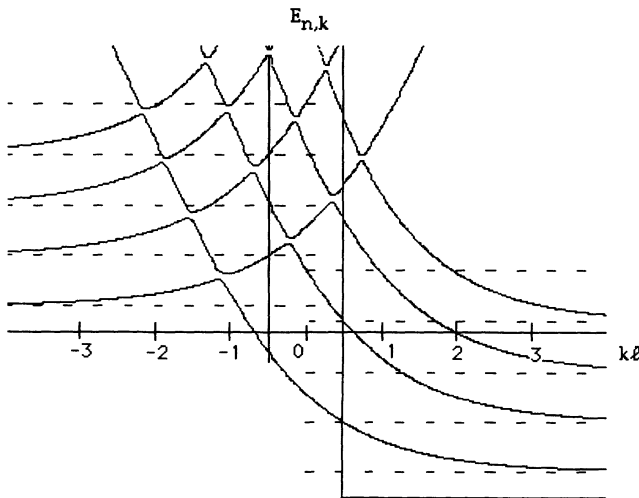


FIG. 10. The spectrum of the entire system in the presence of a voltage bias. The lowest tunneling gap is now moved below the first bulk Landau level.

particle to the left and to the right of the barrier as

$$\begin{aligned} N_L(t) &= \int_{-\infty}^0 dx \hat{\psi}^+(x, y; t) \hat{\psi}(x, y; t), \\ N_R(t) &= \int_0^{\infty} dx \hat{\psi}^+(x, y; t) \hat{\psi}(x, y; t) \end{aligned} \quad (9)$$

the current in x is then $I(t) = e\dot{N}_L = -e\dot{N}_R$. Using the fact that

$$\hat{\psi}(x, y, t) = \sum_{n,k} [L^{-1/2} e^{iky} u_{n,k}(x)] a_{n,k} e^{-iE_{n,k}t/\hbar},$$

we can write

$$\begin{aligned} I(t) &= \sum_k I_k(t) \\ &= \sum_k \frac{ie}{\hbar} \sum_{n,m} [E_{n,k} - E_{m,k}] \\ &\quad \times g_{n,m}(k) a_{n,k}^+ a_{m,k} e^{i[E_{n,k} - E_{m,k}]t/\hbar}, \end{aligned} \quad (10)$$

$$g_{n,m}(k) = \int_{-\infty}^0 u_{n,k}(x) u_{m,k}(x) dx. \quad (11)$$

Note that only terms with $n \neq m$ contribute to the current as $g_{n,m}(k)$ reduces to the overlap of two orthogonal states in L or R in the $V_0 = \infty$ limit,

$$g_{n,m}(k) \approx 0 \text{ for } |k| > 1. \quad (12)$$

For this reason, we can from now on focus on the range $|k| \leq 1$ in Eq. (10).

Limiting to the lowest two Landau levels Eq. (10) becomes

$$I(t) = \sum_k \frac{ie}{\hbar} T_k a_{1,k}^+ a_{0,k} e^{i[E_{1,k} - E_{0,k}]t/\hbar} + \text{H.c.}, \quad (13)$$

$$T_k = [E_{1,k} - E_{0,k}] g_{1,0}(k).$$

For $|k| \leq 1$, Eq. (6) implies

$$g_{1,0}(k) \approx \frac{1}{2} \int_{-\infty}^0 dx [|\phi_{0,k}^L(x)|^2 - |\phi_{0,k}^R(x)|^2] \quad (14)$$

$$= \frac{1}{2} \int_{-\infty}^0 dx |\phi_{0,k}^L(x)|^2 = \frac{1}{2}. \quad (15)$$

With Eq. (15) and Eq. (12), we have

$$T_k \approx (E_{1,0} - E_{0,0})/2 \equiv \Delta_0/2 \text{ for } |k| \ll 1 \quad (16)$$

$$\approx 0 \text{ for } |k| > 1. \quad (17)$$

III. EFFECTIVE TUNNELING HAMILTONIAN AND THE TUNNELING CURRENT

In this section and the next two, we shall focus on the tunneling between the lowest Landau level of L and R . For simplicity, we shall also consider the case of zero bias. The results derived here can be generalized easily to other Landau levels and to nonzero bias. The Hamiltonian of the entire system, Eq. (4), now reduces to

$$H = \sum_k (E_{0,k} a_{0,k}^+ a_{0,k} + E_{1,k} a_{1,k}^+ a_{1,k}). \quad (18)$$

As discussed in Sec. I, only those k 's in the range $|k| \leq 1$ contribute to the current Eq. (10). Within this range, $E_{0,k}$ and $E_{1,k}$ are close to $\epsilon_{0,k}^L$ and $\epsilon_{0,k}^R$ except at $k=0$,

(i.e., the intersection of $\epsilon_{0,k}^L$ and $\epsilon_{0,k}^R$), where a gap Δ_0 is opened up (see also Figs. 8 and 11). For later discussions we define

$$E_{1,k} - E_{0,k} \equiv E_k, \quad \Delta_0 \equiv E_{k=0} = E_{1,0} - E_{0,0}. \quad (19)$$

The tunneling phenomenon contained in Eq. (18) is more transparent if H is written in the form of a tunneling Hamiltonian. Defining energies $\epsilon_{L,k}$, $\epsilon_{R,k}$, and tunneling matrix element T_k as

$$\epsilon_{L,k} - \epsilon_{R,k} = \epsilon_{0,k}^L - \epsilon_{0,k}^R \equiv \epsilon_k, \quad (20)$$

$$\epsilon_{L(R),k} = \epsilon_{0,k}^{L(R)} + \zeta_k, \quad \zeta_k = \frac{1}{2}[E_{1,k} + E_{0,k} - \epsilon_{0,k}^L - \epsilon_{0,k}^R], \quad (21)$$

$$T_k = \frac{1}{2}\sqrt{E_k^2 - \epsilon_k^2}, \quad (22)$$

Eq. (18) can be written as

$$H = H_0 + H_T = \sum_k (\epsilon_{L,k} c_{L,k}^+ c_{L,k} + \epsilon_{R,k} c_{R,k}^+ c_{R,k}) - \sum_k (T_k c_{L,k}^+ c_{R,k} + \text{H.c.}), \quad (23)$$

where

$$\begin{pmatrix} c_L \\ c_R \end{pmatrix}_k = \hat{U}_k \begin{pmatrix} a_0 \\ a_1 \end{pmatrix}_k, \quad \hat{U}_k = \begin{pmatrix} v & u \\ u & -v \end{pmatrix}_k, \quad (24)$$

$$u_k = \left[\frac{1}{2} \left(1 + \frac{\epsilon_k}{E_k} \right) \right]^{1/2}, \quad v_k = \left[\frac{1}{2} \left(1 - \frac{\epsilon_k}{E_k} \right) \right]^{1/2}. \quad (25)$$

The phases of $c_{L,k}$ and $c_{R,k}$ have been chosen so that u_k , v_k , and T_k are all real. [The relation between T_k defined in Eq. (22) and that in Eq. (13) will be clear shortly.] Equation (25) also implies that

$$T_k = u_k v_k E_k. \quad (26)$$

Although, strictly speaking, $\zeta_k \neq 0$, it can be taken as zero as it is much smaller than $\epsilon_{0,k}^{L(R)}$. As a result, $\epsilon_{L,k}$, $\epsilon_{R,k}$, $c_{L,k}$, and $c_{R,k}$ are well approximated by $\epsilon_{0,k}^L$, $\epsilon_{0,k}^R$, $c_{0,k}$, and $d_{0,k}$ [see Eq. (5)], even though they are not exactly the same. H_0 in Eq. (23) can therefore be interpreted as the Hamiltonian of L and R in the infinite barrier limit, and H_T describes the tunneling between them. There is another point worth noting. In the conventional tunneling Hamiltonian, the tunneling term H_T is usually written as $\sum_k (T_k c_{L,k}^+ c_{R,k} + \text{H.c.})$, whereas in Eq. (23) k is conserved during tunneling processes. This is entirely a consequence of the symmetry of the systems in Figs. 2 and 3.

Next, we turn to the tunneling current. Defining the number of particles to the left and to the right as $N_L = \sum_k c_{L,k}^+ c_{L,k}$ and $N_R = \sum_k c_{R,k}^+ c_{R,k}$, the current in x is then $I(t) = e\dot{N}_L = -e\dot{N}_R$, or explicitly,

$$I(t) = \frac{ie}{\hbar} \sum_k [T_k c_{L,k}^+(t) c_{R,k}(t) - \text{H.c.}]. \quad (27)$$

Using Eq. (25) and the fact that $a_{0(1),k}(t) = a_{0(1),k} e^{-iE_{0(1),k}t/\hbar}$, we can write Eq. (27) as

$$I(t) = \frac{ie}{\hbar} \sum_k T_k (a_{1,k}^+ a_{0,k} e^{iE_k t/\hbar} + \text{H.c.}). \quad (28)$$

Using Eq. (25) again, we can rewrite

$$I(t) = \frac{e}{\hbar} \sum_k [v_k(t) (c_{R,k}^+ c_{R,k} - c_{L,k}^+ c_{L,k}) + \eta_k(t) (c_{L,k}^+ c_{R,k} + \text{H.c.})], \quad (29)$$

where v_k and η_k are defined as

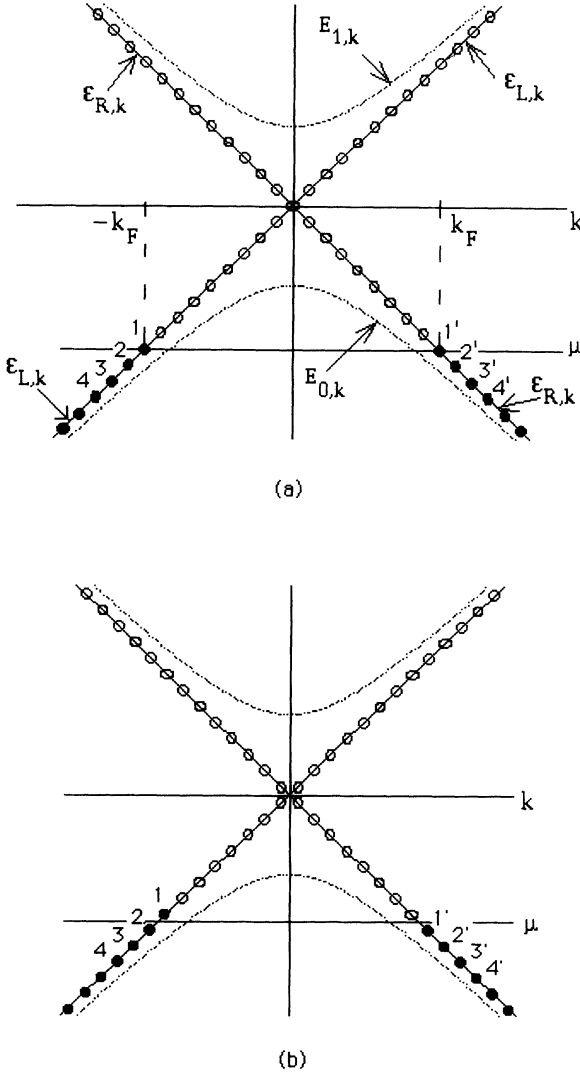


FIG. 11. Both (a) and (b) show the spectrum near the lowest tunneling gap in the region $|k| < 1$. (a) is a schematic representation of the initial state $|\Psi\rangle$ discussed in Sec. IV when both L and R have identical chemical potentials μ . Occupied (unoccupied) states are indicated by solid (empty) circles. The spacing in k is $2\pi/L$. The states $c_{L,k}$ and $c_{R,k}$ are linear combinations of $a_{0,k}$ and $a_{1,k}$. As the boundary condition in y changes (corresponding threading a flux $\theta/2\pi$ through the hole in Fig. 2), all k states move to the right, i.e., 4 and 3 towards 3 and 2, 1' and 2' towards 2' and 3', etc. (b) shows the location of the k states in (a) after half a flux is passed through the hole, i.e., $k \rightarrow k + \pi/L$. This results in an excess edge electron on top of the Fermi surface in L .

$$\begin{aligned} v_k(t) &= 2(T_k u_k v_k) \sin(E_k t / \hbar), \\ \eta_k(t) &= iT_k (e^{iE_k t / \hbar} u_k^2 + e^{-iE_k t / \hbar} v_k^2). \end{aligned} \quad (30)$$

Comparing Eqs. (28) and (26) with Eq. (13), one notes that these two definitions of T_k are consistent if $g_{0,1}$ in Eq. (13) is identified as $u_k v_k$ in Eq. (26). For Eq. (25), one can also see that the asymptotic form Eq. (16) is also satisfied by both definitions.

The expressions Eqs. (28) and (29) represent the major difference between oscillatory tunneling and the usual type of electron tunneling (such as those in normal and Josephson junctions), where first-order perturbation theory in H_T provides an adequate description of the tunneling current,

$$\begin{aligned} I(t) - I(0) &= \frac{i}{\hbar} \int_{-\infty}^t [\tilde{I}(t), \tilde{H}_T(t')] dt', \\ \tilde{A}(t) &\equiv e^{iH_0 t / \hbar} A e^{-iH_0 t / \hbar}. \end{aligned} \quad (31)$$

In the conventional treatment, Eq. (31), higher-order terms corresponding to multitunneling processes are ignored. In contrast, the time dependences in Eqs. (27)–(29) are generated by the full Hamiltonian H , which amounts to extending the perturbation series Eq. (31) to infinite order. (Note that the infinite series is necessary to generate a gap in the spectrum.)

The reason that the perturbative result Eq. (31) is applicable for most systems is because multitunneling processes are usually suppressed by quantum diffusion even in the absence of inelastic scattering. In the usual case, tunneling takes place between electronic states that are extended over the bulk of the sample (L or R). Once tunneled across, the electron leaves the barrier on the time scale of quantum diffusion. The time to travel a distance comparable to the barrier width a/v_F , which is usually much shorter than the tunneling time. As a result, the tunneling current can be accounted for by first order perturbation theory. However, for the junctions we consider, tunneling takes place between edge states which are localized near the barrier. The electron has no where to go after tunneling but to tunnel back. The continuous back and forth tunneling renders the conventional scheme Eq. (31) inadequate.

A simple model. Near the intersection point, one can linearize the infinite barrier spectrum ϵ_k such that

$$\epsilon_k = v_F \hbar k, \quad (32)$$

where v_F is the Fermi velocity which is of the order of $l\omega_c$. When the tunneling is weak, $\Delta_0 \ll \hbar\omega_c$, the region in k space where E_k differs significantly from ϵ_k is $l|k| \leq \Delta_0 / \hbar\omega_c$. We can therefore model E_k as

$$E_k^2 = \Delta_0^2 + \epsilon_k^2. \quad (33)$$

In terms of this model, Eqs. (22) and (26) become

$$T_k = \frac{1}{2} \Delta_0, \quad u_k v_k = \frac{\Delta_0}{2E_k}. \quad (34)$$

IV. OSCILLATIONS OF THE TUNNELING CURRENT

From Eqs. (28) and (29), we see that the tunneling current is made up of different edge state components I_k , each of which oscillates at a different frequency $\omega_k = E_k / \hbar$. In this section, we discuss ways to generate natural current oscillations, and to discuss the dephasing between different current components. For simplicity, let both L and R have identical chemical potentials (i.e., $\mu_L = \mu_R = \mu$), and that μ is below the tunneling gap (see Fig. 11). The corresponding Fermi vectors in L and R are $-k_F$ and k_F , respectively. The quantum state of the system is then $|\Psi\rangle = \prod_{k < -k_F} c_{L,k}^+ \prod_{p > k_F} c_{R,p}^+ |0\rangle$. [That we take the initial state as $|\Psi\rangle$ instead of the true ground state of the entire system $|\Psi_0\rangle = \prod_{|k| > k_F} a_{0,k}^+$ is because the relaxation from $|\Psi\rangle$ to $|\Psi_0\rangle$ requires inelastic processes, which are ineffective when Eq. (1) is satisfied.] The tunneling current is

$$\langle I(t) \rangle = \frac{e}{\hbar} \sum_k v_k(t) (\langle c_{R,k}^+ c_{R,k} \rangle - \langle c_{L,k}^+ c_{L,k} \rangle), \quad (35)$$

where the average is with respect to $|\Psi\rangle$. It is clear that $|\Psi\rangle$ will not generate any current as the current components in L and R cancel each other, $v_k(t) = v_{-k}(t)$, hence

$$\langle I(t) \rangle = \frac{e}{c} \left[\sum_{k < k_F} - \sum_{k > k_F} \right] v_k(t) = 0.$$

The simplest way to generate a single (of a small number of) oscillating current component is to move all the edge states k to the right by a small amount, i.e., shifting k to $(k + \theta/L)$. This shift amounts to changing the periodic boundary condition of the wave function to $\psi(x, y) = e^{i\theta} \psi(x, y + L)$. Returning to the cylindrical geometry Fig. 2, this change of boundary condition corresponds to passing a fraction $(\theta/2\pi)$ of a flux quantum through the center hole. When half of a flux quantum is passed ($\theta = \pi$) we have in effect added an electron on top of the Fermi sea in L (see Fig. 11). The tunneling current is, therefore,

$$\begin{aligned} \langle I(t) \rangle &= -v_{k_F + \pi/L} \approx -v_{k_F} \\ &= -\frac{e}{\hbar} 2(Tuv)_{k_F} \sin(E_{k_F} t / \hbar). \end{aligned} \quad (36)$$

For chemical potentials slightly below the tunneling gap, $lk_F \ll 1$, Eq. (26) implies $(Tuv)_{k_F} = 2E_{k_F} (uv)_{k_F}^2 = E_{k_F}$. We can then write Eq. (36) in a very simple form

$$\langle I(t) \rangle = -e(E_{k_F} / \hbar) \sin(E_{k_F} t / \hbar). \quad (37)$$

If, instead of pushing a flux quantum through L , we introduce a chemical potential difference between L and R at time $t=0$ [$(\mu_L = \mu_R) \rightarrow (\mu_L = \mu + eV/2, \mu_R = \mu - eV/2)$]. The Fermi wave vectors in L and R are then changed to $-k_F + \delta k_F$ and $k_F + \delta k_F$ (see Fig. 12),

$$\delta k_F = eV / (\hbar v_F). \quad (38)$$

The quantum state in Eq. (35) now becomes $|\Psi\rangle = (\prod_{k < -k_F + \delta k_F} c_{L,k}^+) (\prod_{p > k_F + \delta k_F} c_{R,p}^+) |0\rangle$. The cur-

rent at $t > 0$ is then

$$\langle I(t) \rangle = -\frac{e}{\hbar} \sum_{[k]} v_k(t), \quad (39)$$

where $[k]$ denotes the range of excited edge states $|k + k_F| \leq \delta k_F$. Each of the v_k term oscillates with frequency E_k/\hbar . If the entire range $[k]$ lies in the linear region of the spectrum, (hence $E_k \approx \epsilon_k = \hbar v_F k$) (see Fig. 12), then the states at the opposite end of the interval will be the first ones to dephase with each other, as they have a maximum frequency difference. This takes place at time $\tau_{dp}^{(i)} = \hbar / (E'_{k_F} \delta k_F) \approx \hbar / (eV/2)$, referred to as the ‘‘initial’’ dephasing time. As time increases, the coherence of the states in $[k]$ reduces as more and more states at different ends of the interval keep dephasing with each other (see Fig. 12). When $T \sim \tau_{dp}^{(f)} = \hbar / [E'_{k_F} (2\pi/L)] = L / [2\pi v_F]$, referred to as the ‘‘final’’ dephasing time, only one or two states in the vicinity of k_F remain coherent.

During the dephasing period, $\tau_{dp}^{(i)} < t < \tau_{dp}^{(f)}$, the summand in Eq. (39) is sufficiently smooth that the sum can be approximated by the integral

$$\begin{aligned} \langle I(t) \rangle = & -\frac{e}{\hbar} \frac{L}{2\pi} \int_{-k_F - \delta k_F}^{-k_F + \delta k_F} (2T_k u_k v_k) \\ & \times \sin\left[\frac{E_k t}{\hbar}\right] dk. \quad (40) \end{aligned}$$

Expanding the integrand about k_F , Eq. (40) becomes

$$\begin{aligned} \langle I(t) \rangle = & -\frac{e}{\hbar} \frac{L}{2\pi} (2Tuv)_{k_F} \sin(E_{k_F} t / \hbar) \\ & \times \frac{2\sin([E'_{k_F} \delta k_F t] / \hbar)}{E'_{k_F} t / \hbar} + O(t^{-2}) + \dots. \quad (41) \end{aligned}$$

Initially (for $t \approx 0$), Eq. (40) gives

$$\langle I(t) \rangle \approx -\frac{e}{\hbar} (L \delta k_F / 2\pi) (2Tuv)_{k_F} \sin(E_{k_F} t / \hbar), \quad (42)$$

which is the single electron current, Eq. (37), multiplied by the number of electrons that participate in tunneling, $(L \delta k_F / 2\pi)$. The dephasing effect causes this current to decrease as $1/t$ [see Eq. (41)]. At time $t \approx \tau_{dp}^{(f)}$, most of

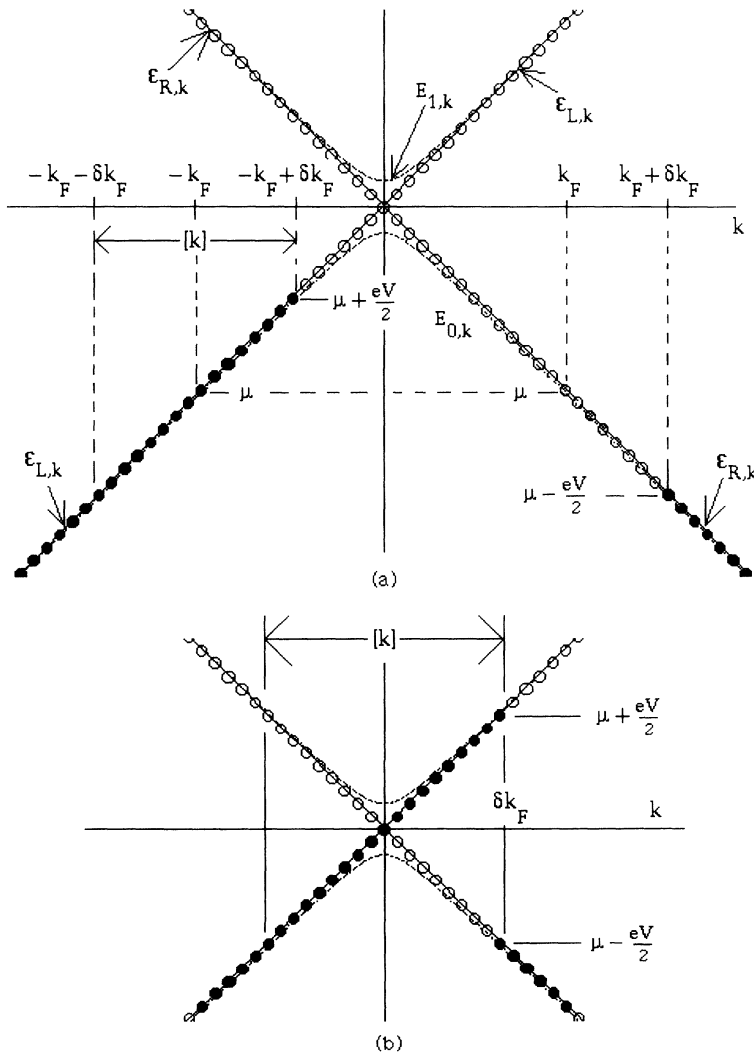


FIG. 12. When a chemical potential difference eV is imposed between R and L at time $t=0$, the Fermi wave vectors in L and R are changed to $-k_F + \delta k_F$ and $k_F + \delta k_F$. The range of k contributing to the tunneling current is given by $|k + k_F| < \delta k_F$, which is denoted as $[k]$. In (a), the range $[k]$ lies in the linear portion of the spectrum. The tunneling current decays as t^{-1} . In (b), $[k]$ includes the intersection point, the tunneling current decays as $t^{-1/2}$.

the terms in Eq. (39) have undergone many oscillations except for a few terms near $k=0$. The magnitude of the current is then reduced to that comparable to a single electron, Eq. (37).

Let us consider a different situation where initially $k_F=0$. The range $[k]$ is then symmetric about $k=0$ (see Fig. 12). The tunneling current, Eq. (39), becomes

$$\langle I(t) \rangle = \frac{2e}{\hbar} \sum_{0 \leq k < \delta k_F} v_k(t). \quad (43)$$

$$\langle I(t) \rangle = -\frac{e}{\hbar} \frac{L}{2\pi} (2Tuv)_{k=0} \int_{-\delta k_F}^{\delta k_F} dk \sin([\Delta_0 + \frac{1}{2}E''_{k=0}k^2]t/\hbar) + O(\dots) \quad (44)$$

$$= -\frac{e}{\hbar} \left[\frac{L\delta k_F}{2\pi} \right] [2\Delta_0 \sin(\Delta_0 t/\hbar)] \sqrt{\pi\hbar\Delta_0/(eV)^2 t} C[\sqrt{(eV)^2 t/\pi\hbar\Delta_0}], \quad (45)$$

where $C(x) \equiv \int_0^x \cos(u^2) du$ is the Fresnel integral which approaches $\frac{1}{2}$ as $x \rightarrow \infty$. In deriving Eq. (45), we have made use of Eq. (38).

From Eq. (45), we can see that as the chemical potential μ sweeps through the gap, the dephasing processes slows down, changing from t^{-1} to $t^{-1/2}$ for large t . The final dephasing time $\tau_{\text{dp}}^{(f)} = \hbar/\delta\omega_{k=0} = (L/2\pi v_F)(\Delta_0/[\hbar v_F(2\pi/L)])$ is much longer than that in the previous case, $(L/2\pi v_F)$, as the factor $\Delta_0/[\hbar v_F(2\pi/L)]$ is typically much larger than 1 (see also Sec. VII).

V. NOISE SPECTRUM

The oscillatory tunneling of the edge states can also be detected through the noise spectrum, $S(\omega) = \int_{-\infty}^{\infty} S(t) e^{i\omega t} dt$, $S(t) = \frac{1}{2} \langle [I(t), I(0)]_+ \rangle$. When both L and R have identical chemical potentials μ , Eqs. (29) and (30) imply that

$$S(t) = \left[\frac{e}{\hbar} \right]^2 \sum_k' \text{Re}[\eta_k^*(t)\eta_k(0)] \\ = \left[\frac{e}{\hbar} \right]^2 \sum_k' |T_k|^2 \cos\left[\frac{E_k t}{\hbar}\right], \quad (46)$$

$$\sum_k'(\dots) \equiv \sum_k(\dots)[f(\epsilon_{L,k})\bar{f}(\epsilon_{R,k}) + f(\epsilon_{R,k})\bar{f}(\epsilon_{L,k})], \quad (47)$$

where $f(x) = (e^{(x-\mu)/k_B T} + 1)^{-1}$ is the Fermi function, T is the temperature, and μ is the chemical potential. The noise spectrum is

$$S(\omega) = \left[\frac{e}{\hbar} \right]^2 \sum_k' |T_k|^2 \pi [\delta(\omega - E_k/\hbar) + \delta(\omega + E_k/\hbar)]. \quad (48)$$

At $T=0$, we have $\sum_k' \rightarrow (L/2\pi)(\int_{-\infty}^{-k_F} + \int_{k_F}^{\infty})$. For $\omega > 0$, we have

The largest frequency difference among different k terms is still eV/\hbar , whereas the minimum frequency difference becomes

$$\delta\omega_{k=0} = (E_{2\pi/L} - E_0)/\hbar \\ = \frac{1}{2}(\hbar^2 v_F^2/\Delta_0)(2\pi/L)^2/\hbar.$$

Therefore, we still have $\tau_{\text{dp}}^{(i)} = \hbar/(eV)$, while the final dephasing time becomes $\tau_{\text{dp}}^{(f)} = 2\pi/\delta\omega_{k=0}$. For $\tau_{\text{dp}}^{(i)} > t > \tau_{\text{dp}}^{(f)}$, Eq. (43) can be written as

$$S(\omega) = \left[\frac{e}{\hbar} \right]^2 L \int_{k_F}^{\infty} |T_k|^2 \delta(\omega - E_k/\hbar) dk \quad (49)$$

$$= \left[\frac{e}{\hbar} \right]^2 L \hbar \left[|T_k|^2 \frac{dk}{dE_k} \right]_{\hbar\omega = E_k} \quad \text{for } \hbar\omega > E_{k_F} \quad (50)$$

$$= 0 \quad \text{for } \hbar\omega < E_{k_F}. \quad (51)$$

Using the simple model at the end of Sec. III, Eqs. (50) and (51) become

$$S(\omega) = \left[\frac{e}{\hbar} \right]^2 \frac{L\Delta_0^2}{v_F} \frac{\omega}{\sqrt{\omega^2 - (\Delta_0/\hbar)^2}} \quad \text{for } \hbar\omega \leq E_{k_F} \quad (52)$$

$$= 0 \quad \text{otherwise.} \quad (53)$$

Note that k_F (hence, E_{k_F}) depends on μ . When μ lies outside the gap, $k_F \leq 0$, and $S(\omega)$ shows a cusp at $\omega = E_{k_F}/\hbar$. When μ lies inside the gap, $S(\omega)$ shows a square root divergence at $\omega = \Delta_0/\hbar$. (See Fig. 13.)

The noise in the tunneling current will generate a similar noise spectrum $S_H(\omega)$ in the Hall current I_H . The Hall current in L is $I_H = L^{-1}(e/\hbar) \sum_k (\partial \epsilon_k^L / \partial k) c_{L,k}^+ c_{L,k}$, and S_H is defined as $S_H(t) = \frac{1}{2} \langle [\delta I_H(t), \delta I_H]_+ \rangle$, where $\delta I_H = I_H - \langle I_H \rangle$. Using Eq. (24), it is straightforward to work out this noise spectrum,

$$S_H(\omega) = \left[\frac{e}{2\hbar L} \right]^2 \left[\frac{L}{2\pi} \right] \int_{k_F}^{\infty} \left[\frac{\partial \epsilon_k}{\partial k} \right]^2 \\ \times (u_k v_k)^2 \pi \delta(\omega - E_k/\hbar), \quad (54)$$

where we have used the fact that $2\epsilon_{L,k} = \epsilon_k$ for unbiased junctions. Using Eqs. (26) and (32), we have

$$S_H(\omega) = \frac{1}{8} \left[\frac{v_F}{L\omega} \right]^2 S(\omega). \quad (55)$$

The noise spectrum of the Hall current is proportional to that of the tunneling current. While $S_H(\omega)$ may be difficult to measure in geometries like Fig. 3, it is easy to measure in the junctions shown in Fig. 5 by measuring

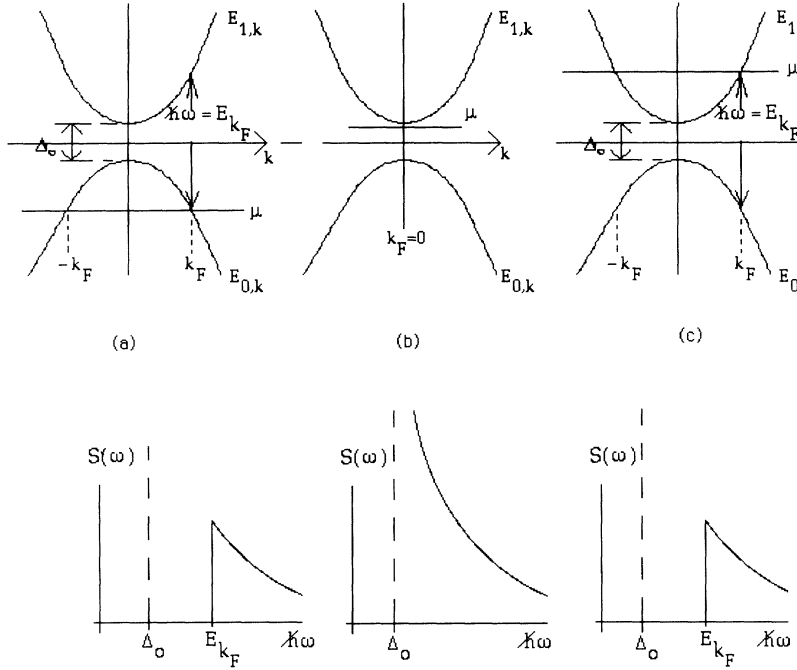


FIG. 13. Noise spectra at different chemical potentials: When μ is below or above the gap, (a) and (c), only states in the range $|k| > k_F$ contribute to the noise. The noise spectrum has a cusp. When μ is inside the gap, all states contribute to the current. The noise spectrum has a square root singularity.

the noise spectrum of the Hall voltage, which is simply $(\hbar/e)^2 S_H(\omega)$. Even though the junctions in Figs. 5 and 3 are not the same, the physics of oscillatory tunneling are identical in both cases. The noise spectrum of the tunneling current in Fig. 5 should have a divergence as any self oscillating system does, which should show up in the noise spectrum of the Hall voltage.

VI. INTERACTIONS BETWEEN EDGE STATES ON DIFFERENT SIDES OF THE BARRIER

So far, we have ignored interactions between edge states on different sides of the barrier. When these interactions are included, the effective Hamiltonian Eq. (23) becomes

$$H = H_0 + H_T + H_{\text{int}}, \quad H_{\text{int}} = \epsilon^{-1} \sum_q U(q) \rho_L(q) \rho_r(-q), \quad (56)$$

where

$$\rho_{L(R)}(q) = \sum_k c_{k+q, L(R)}^\dagger c_{k, L(R)},$$

$$U(q) = \int_{-L/2}^{L/2} e^{-iqy} (4a^2 + y^2)^{-1/2} dy,$$

and ϵ is a dielectric constant. Equation (56) is precisely the massive Thirring model and its spectrum can be solved exactly by the Bethe ansatz.⁵ It is known from the exact solution that there is always a gap in the spectrum for all U . Since the singularities in the noise spectrum and the minimum frequency of the oscillatory tunneling current are due to the existence of the tunneling gap, we expect that these features will persist in the presence of interaction effects.

VII. ESTIMATES OF THE KEY PARAMETERS

Numerical estimates for the parameters in Sec. IV are given in Table I. We shall see from these estimates that

the important condition Eq. (1) is generally satisfied and that the tunneling phenomenon discussed here should be observable for temperatures around 1 K.

In Table I, we have taken $m = 0.067m_e$, where m_e is the mass of the electron. The barrier height has been taken as 1 eV. The tunneling gap Δ_0 is calculated by the quasiclassical method,⁶ and is given by

$$\Delta_0 = \frac{\hbar\Omega}{\pi} e^{-(1/\hbar) \int_{-a}^a |p| dx}, \quad (57)$$

where $2\pi/\Omega$ is a period of the classical trajectory, $\Omega \approx (\frac{3}{2})\omega_c$. The momentum $|p|$ is $p = \sqrt{2m(V_0 - E)} \approx \sqrt{2mV_0}$ since $E \sim \hbar\omega_c$ and $V_0 \gg E$. The dephasing times labeled “linear” and “quadratic” refer to the cases in Sec. VII where the range of $[k]$ states covers the linear and quadratic part of the spectrum (Fig. 12). We see

TABLE I. Parameters in Sec. IV.

	$B = 10 \text{ T}$	
	$2a = 100 \text{ \AA}$	$2a = 60 \text{ \AA}$
$\omega_c \text{ (sec}^{-1}\text{)}$	2.6×10^{13}	2.6×10^{13}
$\omega_c \text{ (eV)}$	1.7×10^{-2}	1.7×10^{-2}
$\omega_c \text{ (K)}$	200	200
$l \text{ (\AA)}$	81	81
$\Delta_0 \text{ (eV)}$	1.2×10^{-4}	6.6×10^{-4}
$\Delta_0 \text{ (K)}$	1.4	7.6
$\Delta_0/\hbar\omega_c$	7.1×10^{-3}	3.8×10^{-2}
$\tau_T \text{ (sec)}$	3.3×10^{-11}	6.3×10^{-12}
$\frac{\hbar v_f}{2\pi}$	7.1×10^{-4}	$1.3 \times 10^{10^{-4}}$
$\frac{\Delta_0}{L}$		
linear $\tau_{dp}^{(f)} \text{ (sec)}$	4.7×10^{-8}	4.7×10^{-8}
quadratic $\tau_{dp}^{(f)}$	1.3×10^{-4}	7.1×10^{-4}

from Table I that Eq. (1) can be satisfied when $\tau_{in} \gg 10^{-11}$ sec. This can be easily achieved since typical values of τ_{in} in the bulk semiconductor at high magnetic field is already about 10^{-8} – 10^{-7} sec around 1 K,⁷ and is expected to be even longer for electron gas in heterojunctions since the density of electron is reduced. Furthermore, since the tunneling gap is of the order of 1.4 K and larger for the parameters we use, the oscillatory tunneling should be observable for temperature around 1 K.

ACKNOWLEDGMENTS

This work was completed during a sabbatical visit to HKUST and CUHK in Hong Kong, and a visit to NHMFL. I thank Nelson Cue, Kenneth Young, Hong-Ming Lai, and Bob Schrieffer for their hospitality. This work was supported by NHMFL through NSF Grant No. DMR 9016241.

*Permanent address.

¹B. Halperin, Phys. Rev. B **25**, 2185 (1982).

²A. H. MacDonald and P. Streda, Phys. Rev. B **29**, 1616 (1984).

³X. G. Wen, Phys. Rev. Lett. **66**, 802 (1991). The Fermi liquid nature of the edge states for the case of integer filling can be derived rigorously using the perturbation method of J. M. Luttinger, Phys. Rev. **121**, 942 (1960); **119**, 1153 (1960).

⁴Because of the condition of Eq. (1), our work also differs from

that of M. Buttiker, Phys. Rev. B **38**, 9375 (1988); T. Martin and R. Landauer, *ibid.* **45**, 1742 (1992).

⁵H. Bergknoff and H. B. Thacker, Phys. Rev. D **19**, 3666 (1979). See also A. Luther, Phys. Rev. B **14**, 2153 (1976) and references therein.

⁶See p. 183 in L. D. Landau and E. M. Lifshitz, *Quantum Mechanics*, 3rd ed. (Pergamon, New York, 1977).

⁷M. Reyzer, J. Low Temp. Phys. **58** (3,4) (1985).

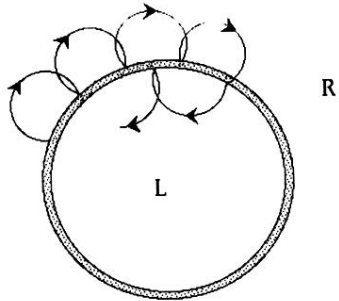


FIG. 1. A quantum Hall junction with a circular barrier. The trajectory of a semiclassical electron is indicated by arrows. Once tunneled across the barrier, the electron will repeat a similar reflected circular motion on the other side and eventually tunnel back.

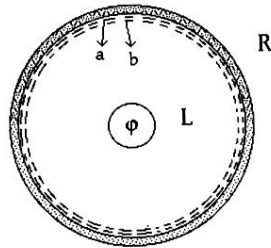


FIG. 2. Schematic representation of the quantum-mechanical edge states near the barrier. The dotted lines labeled a and b denote two neighboring edge states, which in general have different tunneling rates across the barrier. As the flux ϕ through the hole at the center increases, the edge states will move outward, thereby increasing their tunneling rates. State b will evolve to a when $\phi = 2\pi$.

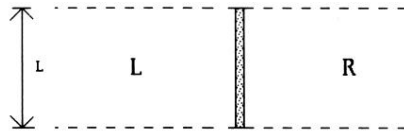


FIG. 3. A rectangular version of the QH junction in Fig. 1. The dashed lines mean that the system is periodic in y with period L .

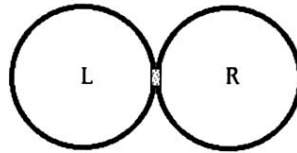


FIG. 4. A quantum Hall weak link. The thick black lines represent hard walls, i.e., infinite potentials. As we shall see, oscillatory tunneling of the electrons across the weak link produces a singularity in the noise of the tunneling current.

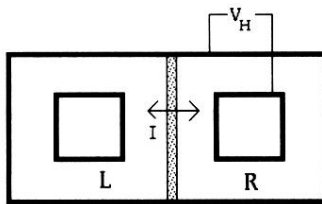


FIG. 5. A junction similar to Fig. 4 except that both R and L are multiply connected geometries. The current oscillation across the junction will generate an oscillation of Hall voltage across each ring.